# Flame-Wall Interaction in Premixed Reactive Turbulence

Peipei Zhao and Lipo Wang
UM-SJTU Joint Institute, Shanghai Jiaotong University
Shanghai 200240, China

Nilanjan Chakraborty
Newcastle University, Newcastle-Upon-Tyne, UK

## 1 Introduction

The modern combustors are often made smaller in size for the sake of increasing the energy-density and improving the compactness but the flame-wall interaction (FWI) becomes a limiting factor. Such interaction may strongly affect the flame structure and the wall cooling. Especially local quenching close to the wall boundary adversely affects the efficiency of the combustors. Therefore, better understanding and rational modeling of FWI are necessary to the engineering design of modern combustion equipments.

In recent years, many efforts have been devoted to the relevant studies. One of the popular FWI configurations is shown in Fig. 1 (a), where the premixed flame propagates toward the cold wall and finally quenches. Based on this configuration, important results, for instance the quenching distance and maximum wall heat flux for both the laminar and turbulent cases, have been obtained [1–3]. Moreover, the local or even global

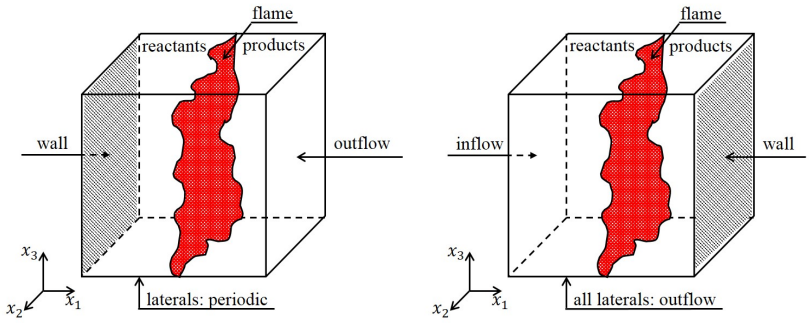


(a) Conventional model (b) New model

Figure 1: The configuration for FWI.

flame structure under the influence of cold wall can also be further investigated. However, in many practical applications the FWI scenario seems to be quite different. Because of the mass and energy transportation by the main stream, the turbulent flame flushes continuously to the solid wall.

Therefore, an alternative FWI configuration is proposed in this work which is schematically shown in Fig. 1 (b). The flame is convected by the inflow with fresh reactants and stopped by the solid wall on the opposite side. The lateral boundaries are set as outflow. In contrast to Fig. 1 (a), here the flame can be stationary and the reactant/product distribution is different. Physically at the stationary state the flame location is balanced with the inflow mass flux, i.e. the incoming flow speed, the fuel consumption rate, i.e. the turbulent flame speed, and the wall boundary condition as well. Roughly in the flame zone the flow can be described by the following one-dimensional conservation relations

$$\rho u_1 = \rho_u u_{1,u} = \rho_b u_{1,b} = \rho_u S_f, \tag{1}$$

and

$$Q_{\dot{w}} = \rho_u u_{1,u} C_p \left(T_b - T_u\right) + Q_{out}, \tag{2}$$

where $\rho$ is the density, $u_1$ is the velocity in streamwise direction, $T$ is the temperature, $S_f$ is the flame speed, $Q_{\dot{w}}$ is the reaction heat release rate, $C_p$ is the specific heat, $Q_{out}$ is the heat transfer rate along the downstream. In the following the subscript '$u$' and '$b$' denote the quantity in the reactant side and product side, respectively. Apparently, when the flame is more closer to the wall, $Q_{out}$ increases.

The objective of the present work is to explore the fundamental physics of FWI in premixed reactive turbulence at the statistically stationary state, based on this new configuration. Especially the adiabatic no-slip wall boundary and isothermal no-slip wall boundary will be compared to understand the FWI properties. In the following, after a brief description of the direct numerical simulation (DNS), we focus mainly on the results and analysis, and end up with concluding remarks.

## 2 Numerical simulations

The three-dimensional compressible reacting flow with the aforementioned configuration in Fig. 1(b) is solved based on the SENGA code [4].The numerical implementation of the spatial derivative adopts a 10th order central difference scheme for the internal points while the scheme order decreases gradually to one-sided 2nd at the boundary points. The three-dimensional characteristic boundary conditions are imposed on the four lateral boundaries. The temporal integration is based on an explicit third-order low storage Runge-Kutta scheme. A steady planar laminar flame solution is prescribed as the initial input [5] into the cubic computational domain with dimension $L_{x_1} = L_{x_2} = L_{x_3} = L = 70\delta_Z$, where $\delta_Z = D_{th}/S_L$ is the Zel'dovich flame thickness with $D_{th}$ and $S_L$ refering to the thermal diffusivity of unburned gas and unstrained laminar flame speed, respectively. The species field is characterized by a reaction progress variable $c = \frac{Y_{R,u} - Y_R}{Y_{R,u} - Y_{R,b}}$, where $Y_R$ is the reactant mass fraction. The non-dimensionalized temperature is defined as $T^+ = \frac{T - T_u}{T_{ad} - T_u}$, where $T_{ad}$ denotes the adiabatic flame temperature. To simplify the complex chemical kinetics, the reaction source adopts a single-step mechanism based on the Arrhenius law, which takes the following form: $\dot{\omega} = B\rho(1-c)exp[-\frac{\beta(1-T^+)}{1-\alpha(1-T^+)}]$, where $B$ is the normalised pre-exponential factor, $\alpha = \dfrac{\tau}{\tau+1}$ with $\tau$ being the heat release number. The characteristic flow parameters and the flame parameters are summarized in the table. 1.

Table 1: Characteristic flow and flame parameters.

| Re | $\mathrm{Pr}_r$ | $Sc_r$ | $Ma_r$ | $\gamma$ | $\tau$ | $\beta$ |
|---|---|---|---|---|---|---|
| 100 | 0.7 | 0.7 | 0.014 | 1.4 | 2.3 | 6.0 |

*The Reynolds number $\mathrm{Re} = \frac{\rho_r u_r l_r}{\mu_r}$, the Prandtl number $\mathrm{Pr}_r = \frac{\mu_r C_{p,r}}{\lambda_r}$, the Schmidt number $Sc_r = \frac{\mu_r}{\rho_r D_r}$, the Mach number $Ma_r = \frac{u_r}{a_r}(a_r = \sqrt{\gamma R_g T_u})$, the ratio of specific heats $\gamma$, the heat release number $\tau = \frac{T_{ad}-T_u}{T_u}$, the Zeldovich number $\beta = \frac{T_a(T_{ad}-T_u)}{{T_{ad}}^2}$ ($T_a$: the activation temperature).

Numerically on the inflow surface, the velocity is specified as the combination of the mean part $U_i$ ($U_1/S_L = 8.0$ and $U_2 = U_3 = 0$) and the fluctuating part $u_i'$ ($u_i'/S_L = 2.0$) by scanning an auxiliary homogeneous isotropic turbulent field generated a priori based on a prescribed energy spectrum. More numerical details can be found in Ref. [4]. Three cases are tested with different no-slip wall boundary conditions (BC) (case A: adiabatic BC, case B: isothermal BC with ${T_{wall}}^+ = 0.5$, case C: isothermal BC with ${T_{wall}}^+ = 0.0$) . In all cases the uniform Cartesian grid size is $256 \times 256 \times 256$, which ensures about 7 grid points per thermal flame thickness $\delta_{th} = \frac{T_b - T_u}{\max(\frac{\partial T}{\partial x})\big|_L}$.

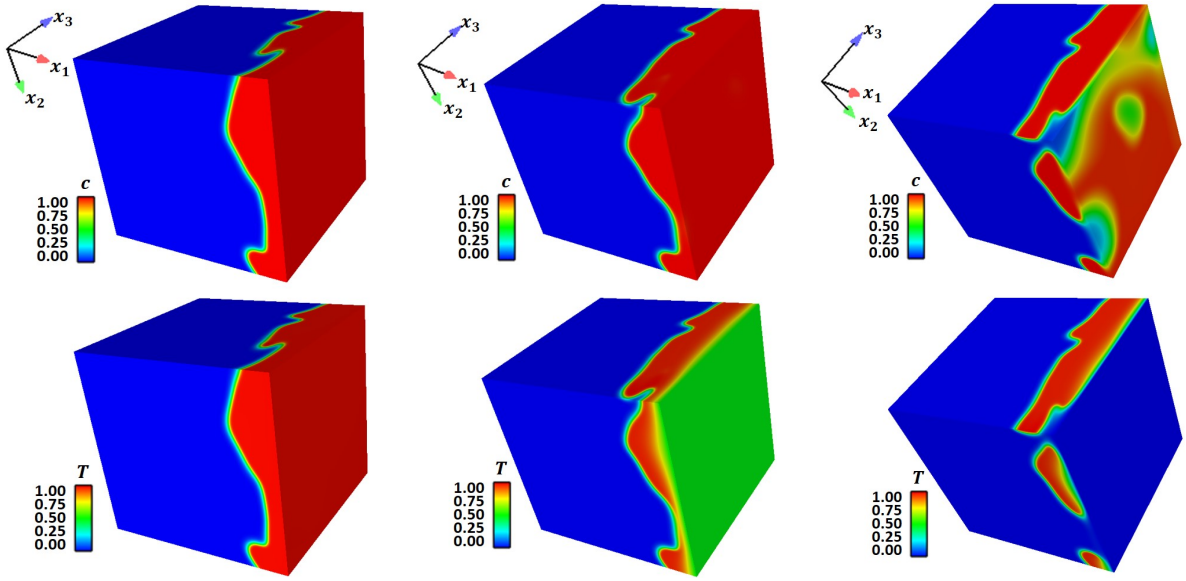


(a) Case A (b) Case B (c) Case C

Figure 2: The flame structure for three cases: adiabatic wall (case A), ${T_{wall}}^+ = 0.5$ (case B) and ${T_{wall}}^+ = 0.0$ (case C).

## 3 Results and analysis

Fig. 2 shows the flame structure for three cases with different wall boundary conditions, once the flow reaches statistical stationary state. With unity Lewis number ($Le = \frac{Sc_r}{\mathrm{Pr}_r} = 1.0$), for case A with the adiabatic wall the reaction progress variable and temperature assume the same spatial structure. In contrast case B and C with cold walls result in the flame closer to the wall. Especially for case C with the lowest wall temperature

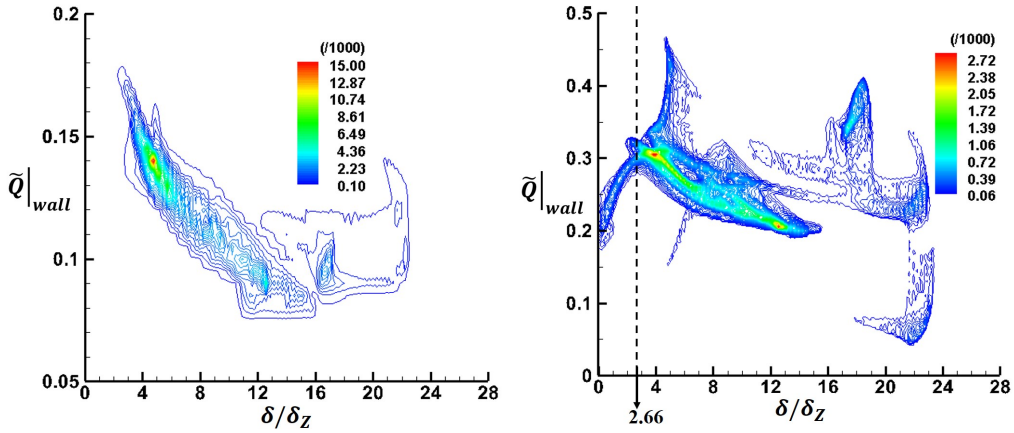


(a) Case B (b) Case C

Figure 3: Joint PDFs between the heat loss to the wall and the flame wall distance for case B & C.

$T_{wall}{}^{+} = 0.0$ the flame becomes broken because of the locally large heat flux to the wall, which then leads to local flame quenching.

For quantitatively analysis, Fig. 3 presents for case B and C the joint probability density function (PDF) between the normalised heat flux to the wall, which is defined as $\tilde{Q}\Big|_{wall} = Q|_{wall}/\rho_r u_r C_{p,r}\,(T_{ad} - T_u)$, and the flame-wall normal distance $\delta/\delta_Z$, which is defined as the straight line along $x_1$ from the $c = 0.85$ isosurface to the cold wall. For case B and C, it shows that the heat flux becomes larger if the distance decreases, as expected. However, because of the lower wall temperature the value of the heat flux for case C is much larger than that for case B. For both cases B and C there is a minimum distance that the $c = 0.85$ isosurface can not go beyond. Moreover, compared with case B, such joint PDF for case C is more structured, especially when the distance is smaller than 2.66, whose physical mechanism will be further explored in the following part. Admittedly, the turbulence in burnt gas decays sharply because of the larger kinematic viscosity in the burnt gas near the wall than the unburnt gas, which lowers the value of heat flux to wall.

Fig. 4 shows the joint PDF between the distance from the flame isosurface ($c = 0.85$) to the wall and the dilatation $\Delta = \frac{\partial u_i}{\partial x_i}$ at the flame surface for three cases. Physically the dilatation is determined by two counteracting mechanisms, the heat generation by reaction and heat loss to the wall. For case A with the adiabatic wall the dilatation at the flame remains to be positive because of the net heat release by reaction. Differently for case B and C the zero dilatation distance is roughly 2.5 and 3.5, respectively, under which the dilatation becomes to be negative because of the excessive wall heat loss. Moreover comparison between Fig. 3 and Fig. 4 presents that for case C there exists a local quenching distance at about 2.66, which is in the same order of quenching Peclet number $P_Q = \frac{\delta_Q}{\delta_Z}$ for the simplified laminar case in Ref. [2]. Physically once the flame quenches, the local heat loss decrease rapidly when the $c = 0.85$ isosurface approaches to the wall; thus the dilatation increases from negative to zero.

In addition to the flame wall interaction, the interaction between flame and turbulence close to the wall is of much importance as well. We consider here the primary alignment relation between the flame normal $\vec{n}$ and the principle axes $\vec{e_1}$, $\vec{e_2}$ and $\vec{e_3}$, which in order correspond to strain rate $s_1 \leq s_2 \leq s_3$, respectively.

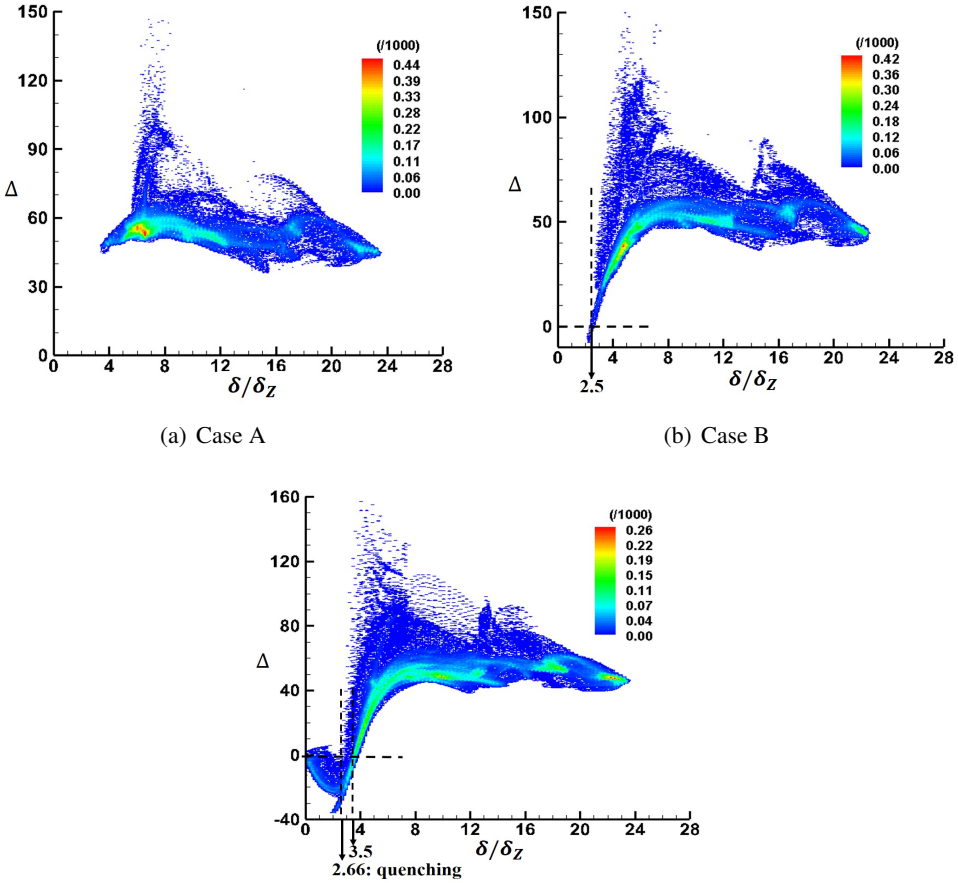


(a) Case A

(b) Case B

(c) Case C

Figure 4: Joint PDFs between the dilatation on the flame and the flame wall distance for three cases.

Fig. 5 shows for the $c = 0.85$ isosurface, the flame normal is preferentially aligned with the most extensive principle axis because of the heat release in the reaction zone, miss-aligned with the intermediate principle axis, and roughly randomly aligned with the most compressive principle axis. Such tendencies are markedly different from the nonreactive case. The results for case B and case C, albeit the influence from heat loss to the cold wall, demonstrate only weak deviation from the case A results, which can be explained by the dominant influences of the flame stretch and the heat loss in the near wall region.

## 4 Concluding remarks

The interaction between the turbulent premixed flame and the solid wall with different boundary conditions has been analyzed. The present counter flow like FWI model demonstrates that the stationary flame interacting with the solid wall is more realistic to understand turbulent combustion in a confined space. If the wall temperature is low enough, the flame surface turns to be broken because of the excessive heat loss to the wall. The flame dilatation is determined by the heat generation by reaction and heat loss to the wall. Roughly the flame quenching distance coincides with the maximum heat loss point. In addition the alignment

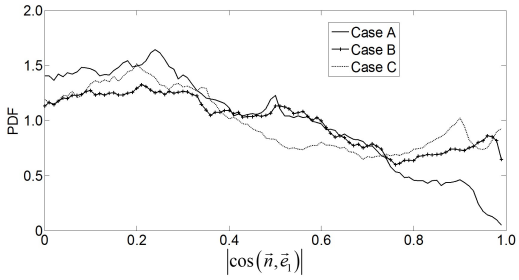


(a) Alignment with the compressive strain direction

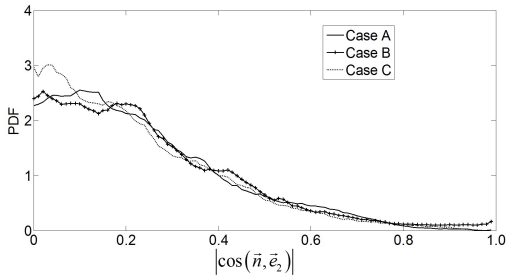


(b) Alignment with the intermediate strain direction

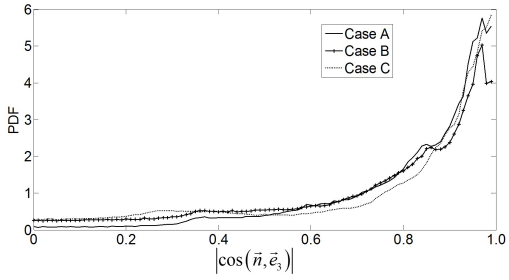


(c) Alignment with the extensive strain direction

Figure 5: PDFs of the alignment between the flame normal and principle strain rate directions ($|\cos(\vec{n},\vec{e}_1)|$, $|\cos(\vec{n},\vec{e}_2)|$, $|\cos(\vec{n},\vec{e}_3)|$) on the flame ($c = 0.85$) for the three cases.

relation between the flame normal and principal axes has also been investigated. The statistics presented here are important to understand the real case of turbulent premixed combustion in confined space, where the effect of the wall boundary condition plays a pivotal role and needs to be considered carefully.

## References

[1] Westbrook C K, Adamczyk A A, Lavoie G A, et al. A numerical study of laminar flame wall quenching[J]. Combustion and Flame, 1981: 81-99.

[2] Poinsot T J, Haworth D C, Bruneaux G, et al. Direct simulation and modelling of flame wall interaction for premixed turbulent combustion[J]. Combustion and Flame, 1993: 118-132.

[3] Lai J, Chakraborty N. Effects of Lewis Number on Head on Quenching of Turbulent Premixed Flames: A Direct Numerical Simulation Analysis[J]. Flow Turbulence and Combustion, 2015, 96(2): 279-308.

[4] K. Jenkins, R. Cant, Direct numerical simulation of turbulent flame kernels, Recent Advances in DNS and LES. Springer Netherlands, 1999: 191-202.

[5] T. Poinsot, D. Veynante, Theoretical and numerical combustion, RT Edwards, Inc., 2005.